ELSEVIER

Journal of Structural Geology 30 (2008) 380–393

JOURNAL OF STRUCTURAL GEOLOGY

www.elsevier.com/locate/jsg

Deformation and kinematics in a melt-bearing shear zone from the Western Betic Cordilleras (Southern Spain)

José Julián Esteban, Julia Cuevas, Néstor Vegas, José M. Tubía*

Departamento de Geodinámica, Facultad de Ciencia y Tecnología, Universidad del País Vasco, Apartado 644, 48080 Bilbao, Spain

Received 12 March 2007; received in revised form 16 November 2007; accepted 21 November 2007
Available online 4 December 2007

Abstract

This work deals with the structural evolution and kinematics of the basal dynamothermal aureole of the Ronda peridotites, located in the Sierra Bermeja massif of the Western Betic Cordilleras, in southern Spain. This aureole is characterized by: 1) a marked strain gradient towards the contact with the overlying peridotites; 2) the great angular dispersion, ≈90°, of stretching lineations; and 3) the intrusion of thin syn-kinematic granite sheets. These features are consistent with the aureole being a low-viscosity shear zone formed at temperatures high enough, ≈725 °C, to promote the partial melting of crustal metamorphic rocks. The high-temperature deformation is demonstrated by the activation of *c*-slip in quartz. We consider that the heat source came from the thrusting of the hot subcontinental mantle over metamorphic crustal rocks. The interaction of alternating events of melt-enhanced deformation and melt-enhanced embrittlement explains the heterogeneity of this ductile shear zone and the strong narrowing, to only 30 meters, of the deformed domain. The small thickness of this shear zone is in contradiction with classical conceptual models of shear zones suggesting a broadening of ductile shear zones with increasing depths and temperatures.

Keywords: Shear zone; Melts; Ronda peridotites; Betic Cordilleras

1. Introduction

Ductile shear zones are common structures in the internal zones of orogens. These structures represent an efficient mechanism of mass transfer and provide clues as to how the lithosphere becomes transformed in the course of orogenic cycles, yet our understanding of the rheological processes involved in the activation of ductile shear zones remains incomplete (Rutter et al., 2001). Probably for these reasons, many works have been published trying to explain the structural evolution (Sibson, 1977; Ramsay, 1980; Platt and Behrmann, 1986) or the processes involved in the nucleation and propagation of ductile shear zones (Passchier, 1986; Blenkinsop, 2000). In the light of the results from such studies, heterogeneity at all scales emerges as an outstanding feature of ductile shear zones.

Nowadays, a growing literature is focussed on the interactions between deformation in ductile shear zones, high-temperature metamorphism and partial melting since these processes work together at deep crustal levels during orogenesis (Mancktelow, 2006). Although field (Hollister and Crawford, 1986) and laboratory studies (Van der Molen and Paterson, 1979; Katz et al., 2006) have shown that the presence of melt favours the localization of ductile shear zones, some controversy remains on the role of melts. In any case, the presence of melts increases the heterogeneity of the shear zones, as melt-enhanced deformation can be balanced by brecciation promoted by melt-enhanced embrittlement (Davidson et al., 1994). As proposed by Brown and Solar (1998) the competition between weakening and embrittlement processes probably reflects that deformation and partial melting interact through positive feedback cycles.

This work compiles observations about the interactions among high-temperature metamorphism, partial melting, emplacement of granite magmas and deformation from the

* Corresponding author. Tel.: +34 9 4601 5392; fax: +34 9 4601 2470.
E-mail address: jm.tubia@ehu.es (J.M. Tubía).

0191-8141/$ - see front matter © 2007 Elsevier Ltd. All rights reserved.
doi:10.1016/j.jsg.2007.11.010

basal shear zone of the Ronda peridotites, located in the western corner of the Alpujarride Complex of the Betic Cordilleras, in southern Spain (Fig. 1). The selected region is a good target to examine these questions because the emplacement of the peridotites is related to a high-temperature shear zone and partial melting in the underlying crustal rocks. We will show that the combination of high-temperature conditions and partial melting promoted the formation of a low-viscosity, narrow shear zone preventing the ascent of significant amounts of granite magma and provides an explanation for the heterogeneous kinematics of the shear zone.

2. Regional setting

The studied region is located in the western part of the Betic Cordillera, in southern Spain (Fig. 1). The Betic Cordillera is the westernmost belt of the peri-Mediterranean Alpine orogen and was formed during the convergence of the African and Iberian plates from Late Cretaceous to Tertiary times (Dewey et al., 1989). The Internal Zone, also known as the Betic Zone (Egeler and Simon, 1969), shows mainly metamorphic rocks of Palaeozoic and Triassic age distributed in three main tectonic complexes that are, in ascending order, the Nevado-Filabride, Alpujarride and Malaguide.

The Ronda peridotites (Fig. 1), the largest worldwide exposure of subcontinental lithospheric mantle, are mainly composed of plagioclase and spinel lherzolites with subordinate garnet lherzolites towards the top of the ultramafic body (Obata, 1980) and minor dunites and harzburgites. The Ronda peridotites form the lower portion of the Los Reales nappe, the highest unit of the Alpujarride Complex in the Western Betics (Tubía et al., 1992). The Los Reales nappe is a composite thrust sheet (Tubía et al., 1997) that includes a lower portion of subcontinental mantle —the Ronda peridotites —and an overlying crustal sequence with kinzigites, migmatite gneisses, and medium-to-low grade metapelites and metapsammites on the top. The Los Reales metamorphic sequence shows isograds that trend roughly parallel to the lithological contacts and to the regional foliation. The Ronda peridotites are emplaced over the Guadaiza and the Ojen nappes. These two nappes have a typical Alpujarride lithological sequence with metapelites at the bottom and Triassic marbles on the top (Navarro-Vilá and Tubía, 1983) but the Ojen nappe recorded high-pressure metamorphic conditions with eclogites (Tubía and Gil Ibarguchi, 1991) whereas the Guadaiza nappe exhibits only low-pressure metamorphic conditions. The hot emplacement of the Ronda peridotites produced a dynamothermal aureole, mainly formed by diatexites and cordierite-bearing migmatites, strongly mylonitised during the overthrusting of the peridotites (Lundeen, 1978; Tubía and Cuevas, 1986). This dynamothermal aureole is concordant with the peridotite contact and originated during the Alpine Orogeny (Tubía and Cuevas, 1986; Sánchez Rodríguez and Gebauer, 2000).

3. Geology of the Guadaiza nappe

The Guadaiza nappe crops out in two main areas, the Albornoque sector to the east, and the Guadaiza tectonic window, surrounded by the overlying Ronda peridotites to the west. Minor outcrops are found in the northern part of the studied region, as small windows within the peridotite massif and along the thrust contact between the Ronda peridotites and

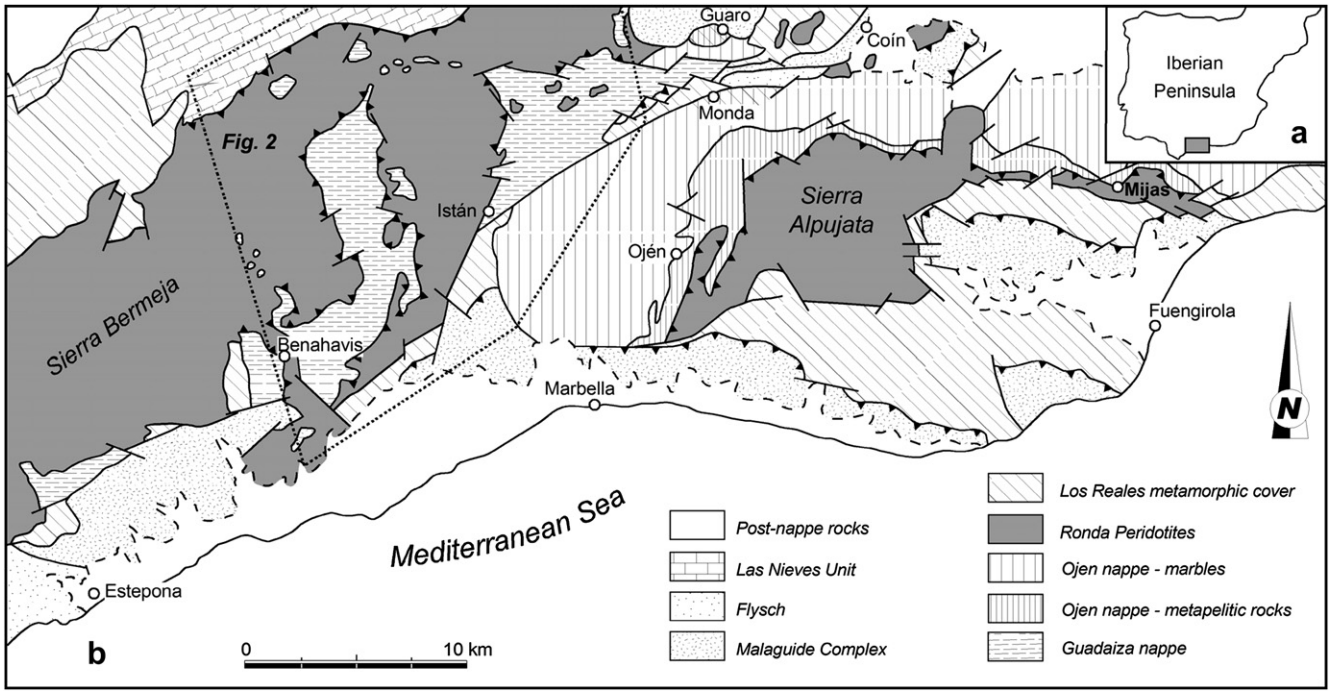

Fig. 1. (a) General location of the studied area within the Iberian Peninsula. (b) Simplified tectonic map of the western part of the Betic Cordillera (modified from Navarro-Vilá and Tubía, 1983). The dashed polygon indicates the location of Fig. 2.

the Triassic limestones (locally marbles) of the Sierra de Las Nieves (Fig. 2). Fig. 3 represents a synthetic log of the Guadaiza nappe. The lowest materials are the Istan migmatites, which are overlain by a metapelitic sequence with interlayered quartzites, schists and minor amphibolites. Coarse-grained marbles complete the lithological sequence and are locally abundant to the southwest of the Guadaiza tectonic window (Fig. 2).

The Istan migmatites, defined by Tubía (1988), include gneisses, diatexites, metatexites and medium to fine-grained leucogranites. The gneisses are composed of K-feldspar + biotite + sillimanite + quartz + plagioclase ± garnet. Centimetric disharmonic folds deform the layering of the gneisses. A poorly developed stretching lineation and symmetric strain shadows around K-feldspar porphyroblasts suggest oblate strain. As the lower contact of the Istan migmatites is not exposed, only a minimum thickness of 150 meters can be estimated for these materials. The leucogranites are concentrated in the NW part of the Istan migmatite domain and their contact with the overlying metamorphic rocks is intrusive.

In the schists and quartzites the metamorphic conditions range from the andalusite zone at upper levels to the sillimanite zone close to the contact with the Istan migmatites. Two distinctive features of this part of the sequence are the abundance of folded veins of quartz and a widespread alteration that is recognized by the dark brown colour of the overall lithological sequence in the field (Fig. 4a). These rocks contain a well-developed planar fabric, S_2, defined by aligned micas, sillimanite, flattened quartz grains and ribbons of white quartz, frequently boudinaged. Minute inclusions of biotite, graphite and garnet within porphyroblasts of plagioclase and staurolite define internal foliations with sigmoidal patterns. Such internal foliations are frequently in continuity with the external S_2 foliation, pointing to the synkinematic growth of the porphyroblast and to a deformation with a rotational component. Andalusite and some biotite are late kinematic and the garnet is scarce and residual.

Two anatectic events have been recognized in the Guadaiza nappe from field arguments (Tubía, 1988). The oldest is recorded by the Istan migmatites and related to the regional

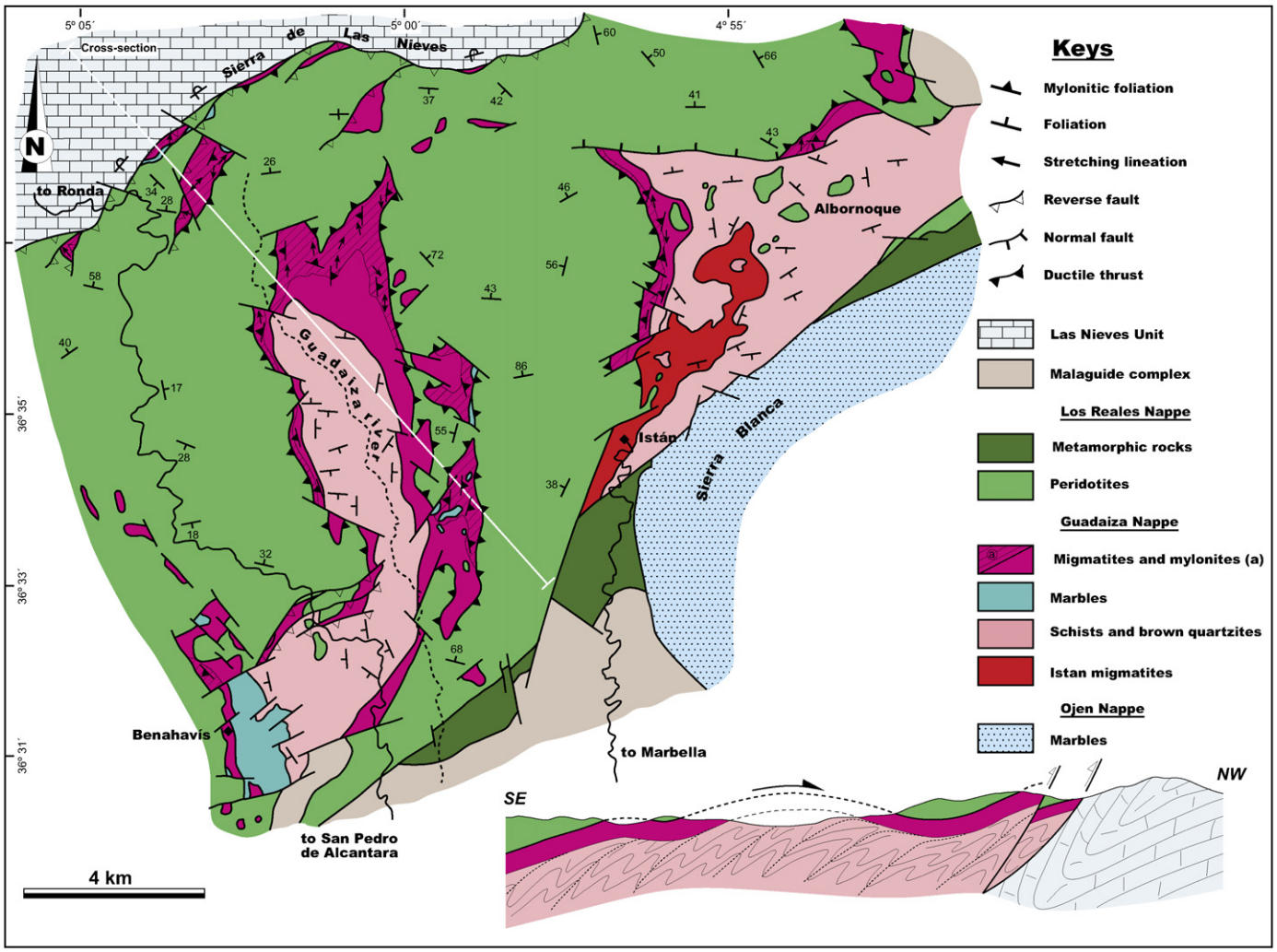

Fig. 2. Geological map of the eastern part of the Sierra Bermeja massif showing the Albornoque sector and the Guadaiza tectonic window. The NW–SE cross-section across the Guadaiza tectonic window explains the structural relations between the peridotites and the underlying rocks, the dynamothermal aureole (undifferentiated) and the schists and brown quartzites.

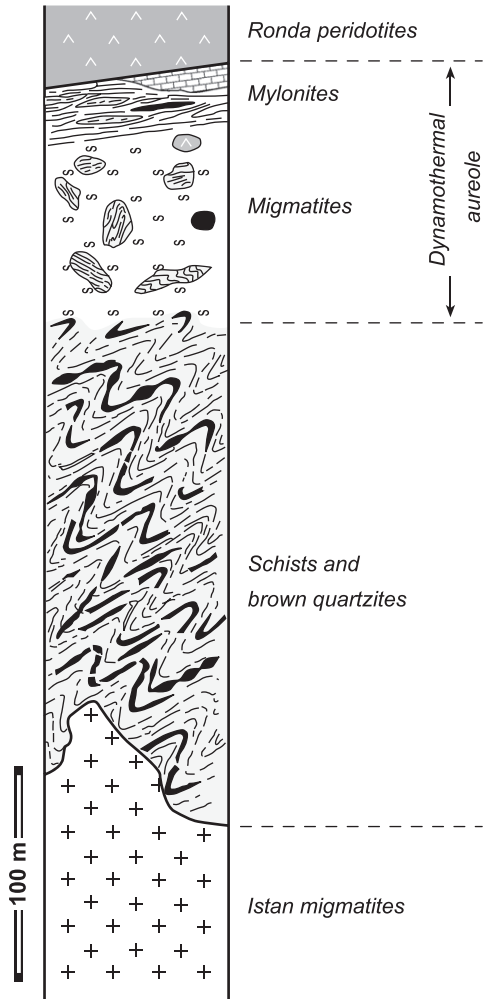

Fig. 3. Synthetic log of the Guadaiza nappe, modified from Tubía (1988). Note the position of the Istan migmatites and the migmatites belonging to the dynamothermal aureole below the peridotites.

metamorphism, while the youngest event is represented by migmatites concentrated in a dynamothermal aureole associated with the overlying Ronda peridotites (Fig. 3). According to geochronological studies with the $^{207}Pb/^{206}Pb$ sequential evaporation technique (Acosta, 1997) and U/Pb SHRIMP dating of zircons (Sánchez Rodríguez, 1998), Hercynian ages of 319 ± 8 Ma and 299 ± 4 Ma, respectively, have been found for the first migmatisation event. In contrast, the second migmatisation event is of Alpine age, ≈22 Ma (Sánchez Rodríguez, 1998). In the following sections we will describe the dynamothermal aureole related to the Alpine migmatisation event.

3.1. Dynamothermal aureole

In contact with the overlying peridotites, there is a continuous layer, 100–200 meters thick and mainly formed by migmatites (Fig. 3), which is interpreted here as a dynamothermal aureole developed from the metapelitic sequence of the Guadaiza nappe. This aureole obliquely cuts the remaining materials of the Guadaiza nappe, resting discordantly on the marbles at the southwestern side of the Guadaiza window and on the Istan migmatites in the Albornoque sector (Fig. 2). Generally, the anatexis increases toward the peridotite contact. The lower portion of the aureole contains stromatic migmatites that are progressively replaced by medium-to coarse-grained nebulites rich in angular restites (Fig. 4b) from the metapelitic sequence and rounded blocks of white quartz (Fig. 4c). Large resisters of marble, some of them of hectometric length, are common and even angular xenoliths from the overlying peridotites are observed in a few places. The uppermost part of the aureole is strongly deformed, with mylonitic rocks. In fact, mylonites with S–C structures can be recognized (Fig. 4d) and both the metapelitic restites and the quartz blocks have acquired ellipsoidal shapes and contribute to define the mylonitic foliation (Fig. 4e). Sometimes, undeformed granite dykes traverse the mylonitic foliation (Fig. 4f) suggesting that partial melting events and solid-state deformational events interacted each other repeatedly. The intrusion of the leucocratic dyke swarm in the Ronda peridotites has been related to the same deformational event described here for the mylonites of the Guadaiza nappe (Cuevas et al., 2006).

This migmatite band has some mineralogical differences, depending on whether they contain restites or not. When restites are absent, the mineral association is quartz +K-feldspar + plagioclase + biotite + cordierite + tourmaline ± sillimanite, generally with idiomorphic plagioclase crystals. A distinctive feature is the replacement of restitic andalusite by prismatic sillimanite or by cordierite (Fig. 5a). These observations point to a notable increase of temperature and moderate increase of pressure conditions during the aureole formation. When these migmatites contain restites the mineral associations are similar, but there are some differences such as a higher proportion of mafic minerals, a generalized presence of garnet included in the K-feldspar and a more calcic plagioclase. The cordierite, which shows twinning and zoning, includes sillimanite (Fig. 5b) and biotite and indicates a simultaneous growth for the three minerals. Generally, the Al-rich restites develop reaction borders of cordierite and hercynite spinel formed from earlier sillimanite and garnet. These borders mark in dark green the contour of these xenoliths in the migmatite country rock.

4. Structural chronology and directional data

The Guadaiza nappe preserves metamorphic and deformational events previous to the emplacement of the Ronda peridotites. On the basis of mapping and new structural data, we have recognized two major deformational events older than the formation of the dynamothermal aureole. The oldest event, D_1, is usually preserved as a residual schistosity in quartz-rich layers crenulated by microfolds (Fig. 5c) associated with the subsequent deformational event. This early schistosity is parallel to the veins of white quartz and also parallel to the lithological contacts. A younger deformational event, D_2, produced tight folds of S_1 with a penetrative axial planar foliation, S_2, defined by the parallel orientation of the main mineral associations. This penetrative foliation vanishes

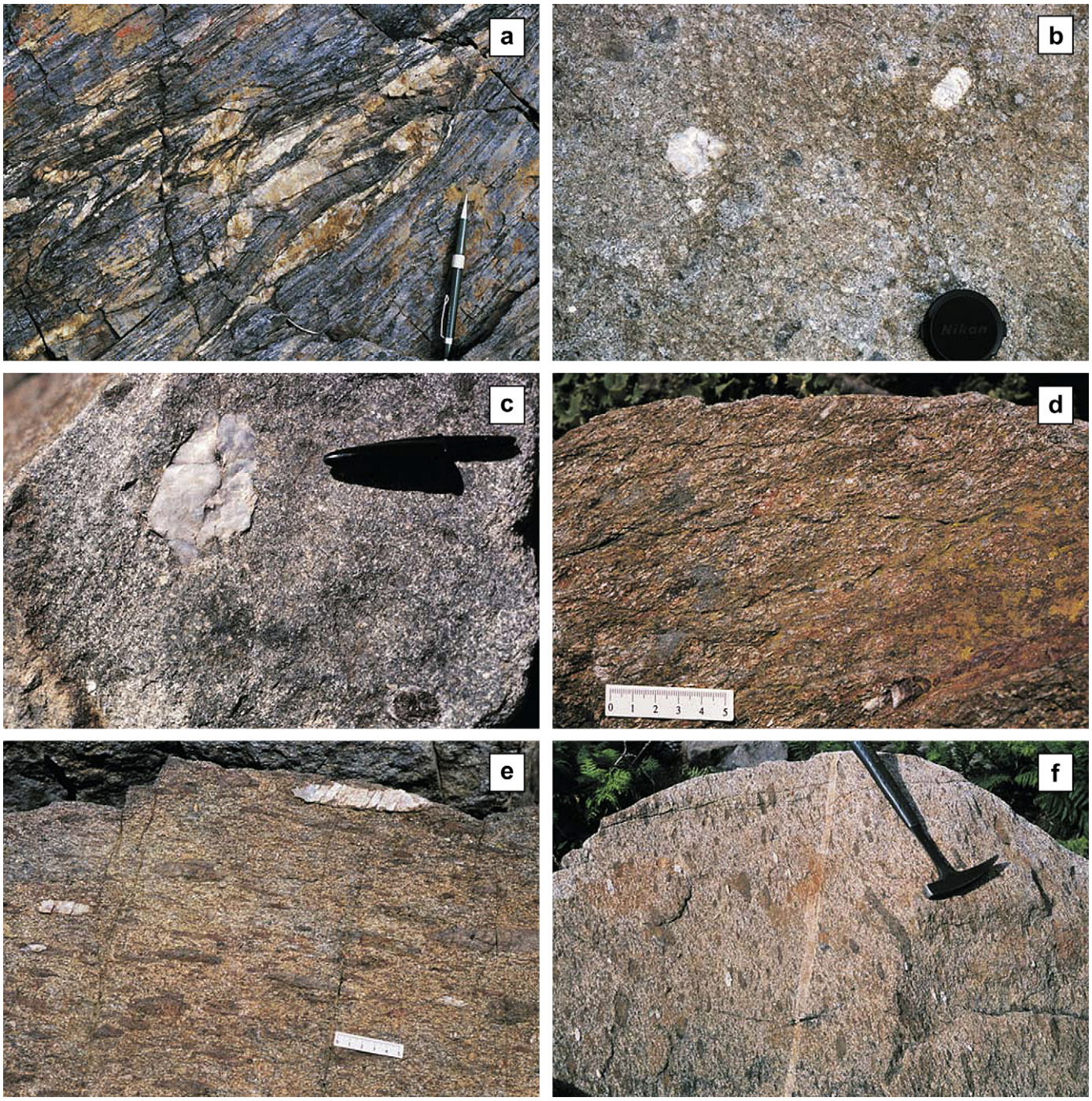

Fig. 4. Outcrop views of the Guadaiza nappe rocks. (a) Asymmetric folded veins of quartz located within the schists and brown quartzites. (b) Undeformed migmatite with nebulitic texture. Note undeformed quartz blocks (white) and metapelitic enclaves (dark) (c) Rounded white quartz block from an undeformed nebulitic migmatite. (d) Mylonite with S–C structures. (e) Mylonitic migmatite with oriented metapelitic enclaves and elongated blocks of white quartz. Note the antithetic microfaults developed in the quartz blocks (f) Mylonitic migmatite cut by a late granite vein.

towards the contact with the peridotites, and can only be observed in the resisters of the dynamothermal aureole.

Based on the variable trend of the main foliation, S_2, two structural domains can be differentiated within the schists of the Guadaiza nappe. In the Albornoque sector the strike of the penetrative foliation is ENE and dips to the SSE (Fig. 6a), as it commonly does elsewhere in the Alpujarride Complex (Tubía et al., 1992). However, within the northern part of the Albornoque sector S_2 is concordant with the basal and N-dipping contact of the Ronda peridotites (Fig. 2), which suggests a dragging effect of the main schistosity of the Guadaiza nappe during the tectonic emplacement of the ultrabasic slab. The second sector corresponds to the Guadaiza window, where the stereoplot of poles to S_2 (Fig. 6b) shows

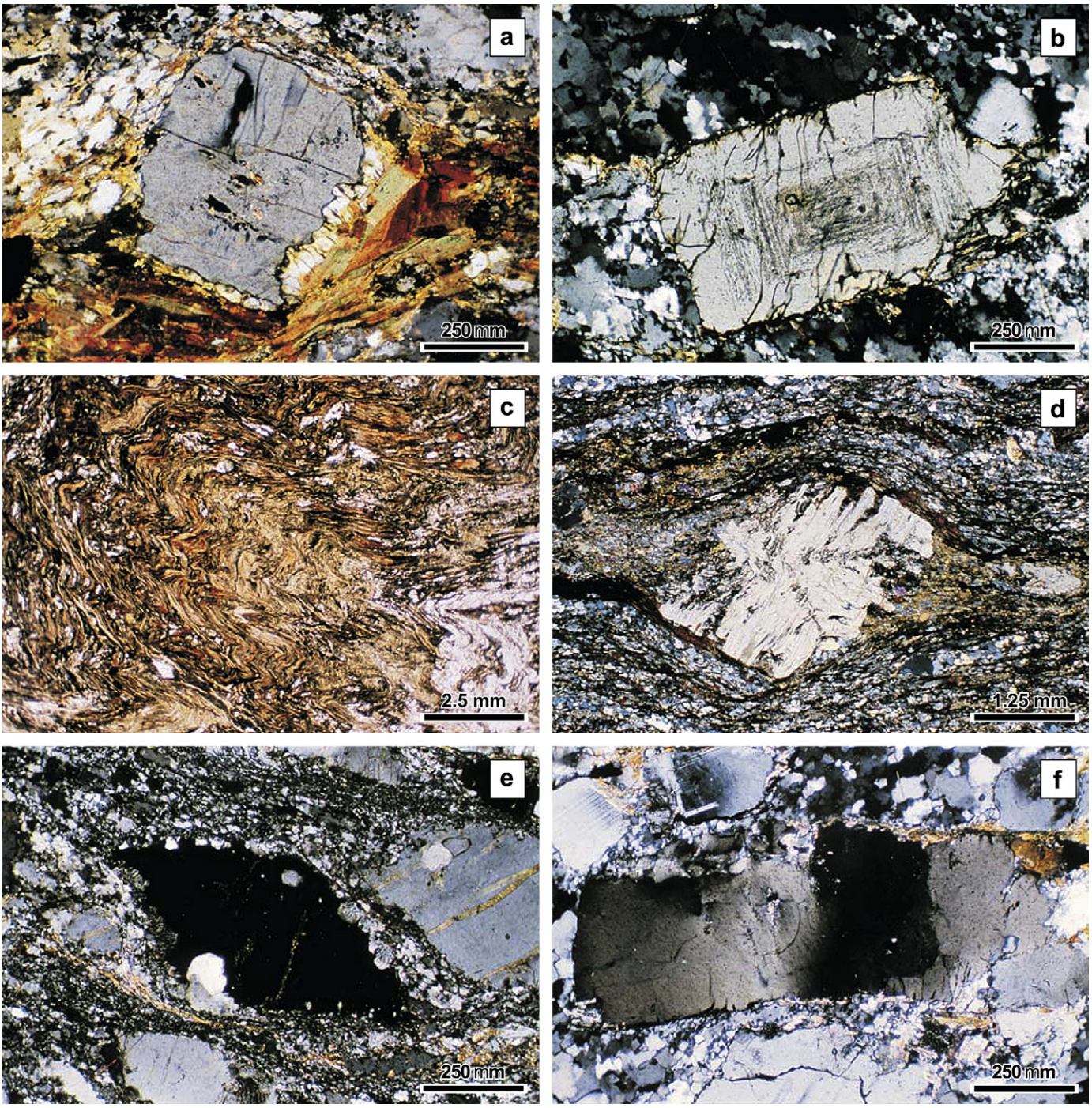

Fig. 5. Photomicrographs of Guadaiza nappe rocks. (a) Andalusite porphyroblast with cordierite overgrowth in a mylonitised migmatite. (b) Mylonitic migmatite with a slightly pinnitized cordierite crystal with epitactic microstructure inclusions of prismatic sillimanite. (c) Residual asymmetric microfolds of D_2 in schists. (d) Mylonitic migmatite with a σ-type porphyroclast of andalusite (e) Mylonitic migmatite with a σ-type porphyroclast of K-feldspar with asymmetric distribution of myrmekites. (f) Elongate cordierite crystal with kink-band boundaries arranged at high angles to the mylonitic foliation and an elongated and boudinaged plagioclase crystal.

that the schists outline a gentle N–S antiform with a roughly N-striking and steeply dipping axial surface. Since the axis of this antiform and the dominant dip of S_2 in the Albornoque sector display similar plunges to the SSE, we interpret this fold as a late structure developed from previously deformed rocks with a mean orientation of S_2 similar to that of the Albornoque sector. This late antiform is also consistent with the N–S elongation of the Guadaiza window (Fig. 2).

The stromatic and nebulitic rocks of the dynamothermal aureole are devoid of synkinematic folds, the most useful structures to establish the relative chronology of deformational processes in migmatites (see Hopgood, 1999). However, the

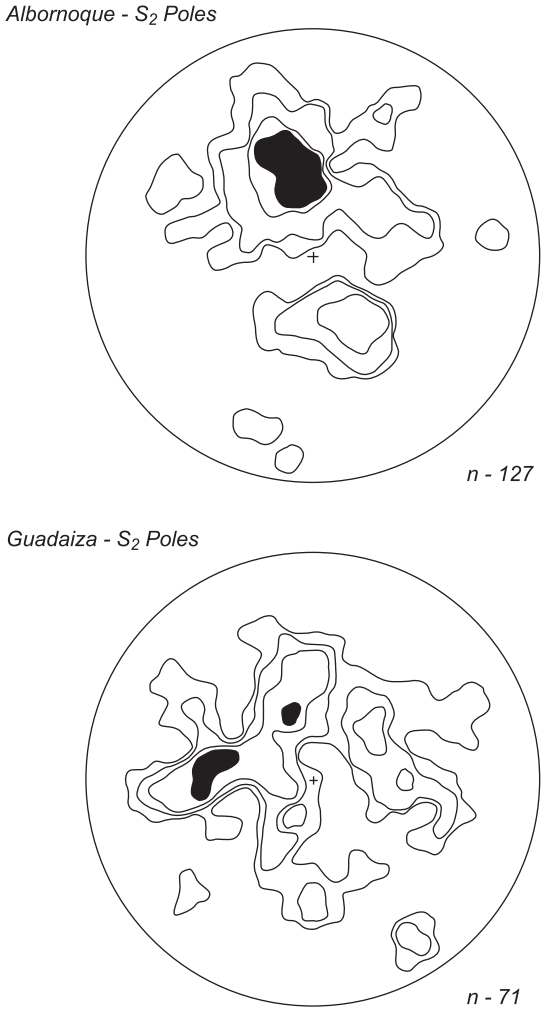

Fig. 6. Stereographic plots of the foliation poles to S_2 of the schists and brown quartzites from Albornoque sector (a) and Guadaiza tectonic window (b). Equal area projections, lower hemisphere. Contours at 1, 2, 4 and 8%; *n* is the number of measurements.

dynamothermal aureole is characterized by a strong gradient of deformation increasing towards the contact with the Ronda peridotites. The strain-free migmatites located in the lowest portion of the aureole (Fig. 4b) are progressively transformed into protomylonites that give way to S–C mylonites (Fig. 4d) and, finally, there are ultramylonites with a penetrative mylonitic foliation close to the peridotites (Figs. 4e,f). The strain gradient is also evident from the shape and orientation of the restites and resisters included in the migmatites, as they display angular and roughly equiaxial shape and are randomly orientated in the strain-free migmatites but are elongate and parallel to the mylonitic foliation in the deformed domain (compare Figs. 4c,e). The transition from the strain-free migmatites to the ultramylonites in contact with the peridotites takes place in a narrow zone, only 30 meters thick. On the mylonitic foliation, a lineation can be clearly recognized due to the marked elongation of the enclaves, which provide *X*/*Y* ratios ranging from 3.56 in the metapelitic restites to 2.48 in the quartz blocks. The elongation of the enclaves is parallel to the mineral lineation defined by the porphyroclasts of K-feldspar and cordierite or by quartz ribbons. Several criteria, like the development of antithetic microshear zones in elongate blocks of quartz (Fig. 4e), demonstrate the stretching nature of the lineation.

The poles of the mylonitic foliation (Fig. 7) are grouped in a partial girdle that represents the profile of the late, vertical and N–S trending antiform. While the axis of the antiform defined by the mylonitic foliation plunges 12°/350° (Fig. 7), the axis of the late fold drawn by the underlying schists is 20°/170° (Fig. 6b). The resulting angular variance implies that the mylonitic zone, and hence the basal contact of the Ronda peridotites, cuts obliquely across the older structures of the Guadaiza nappe. The stretching lineation shows a dominant NNW trend although it is characterized by a great dispersion within the NW to NE quadrangle (Fig. 7). Most of the mylonites crop out in the Guadaiza window (Fig. 2) and probably for this reason the measurements of the stretching lineation reproduce the two great circles corresponding to the limbs of the late N–S antiform (Fig. 7). It is worth noting, however, that the dispersion of lineations cannot be justified by the late N–S folding alone, because if such late folding is restored a dispersion of more than 70° still persists (Fig. 7). This result is consistent with field observations showing that even in areas smaller than 0.001 km^2, where the mylonitic foliation displays a uniform orientation, the lineation defines fan-like distributions of 90° around a dominant N10°W trend. Taken together these observations indicate that the dispersion of the lineation is a primary structural feature related to the mechanism of deformation leading to the formation of the dynamothermal aureole.

Kinematic criteria used to determine the shear sense of the dynamothermal aureole include the S–C structures (Fig. 4d), antithetic microfaults of elongate blocks of quartz (Fig. 4e) and K-feldspar porphyroclasts, the asymmetry of σ-porphyroclasts (Fig. 5d), the asymmetric distribution of myrmekites in K-feldspar

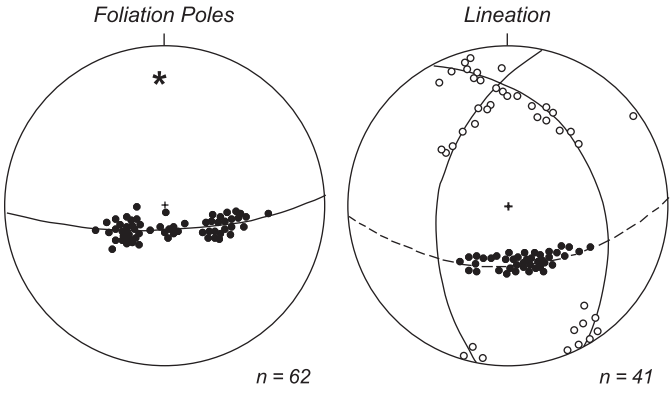

Fig. 7. Mylonitic foliation poles of the dynamothermal aureole to the Guadaiza nappe. Equal area projection, lower hemisphere. The poles of foliation define a girdle that represents the profile of an antiformal fold whose axis plunges 12°/350° (star). Stretching lineation diagram of the dynamothermal aureole to the Guadaiza nappe. Equal area projection, lower hemisphere. The stretching lineations (white dots) are distributed along two great circles that coincide with the average orientations of the mylonitic foliation. Black dots represent the orientation of those stretching lineations after the antiform has been restored to the horizontal.

porphyroclasts (Fig. 5e), the obliquity of microkinks in porphyroclasts (Fig. 5f) and the shape foliation in quartz ribbons. The dominant sense of shear is top to the North (top to the NE or to the NW for lineations displaying such trends).

In order to constrain the deformation conditions we have analysed the microstructure and fabric of quartz in stretched resisters of quartz, as in this mineral the switch from basal $\langle a \rangle$ to prism [c] slip is mainly controlled by the temperature (Mainprice et al., 1986; Kruhl, 1996; Stipp et al., 2002). Fig. 8 documents the microstructure and c-axis diagrams of three samples collected in mylonitic bands between 5 and 30 m from the peridotite contact. In XZ sections all the samples are composed of recrystallized grains with chessboard patterns. The grains of quartz show square to rectangular shapes with grain boundaries at right angles and asymmetrical to the trace of the mylonitic foliation (Fig. 8a). Basal subgrain boundaries are developed (Fig. 8b). The diagrams of crystallographic preferred orientation of c-axis are characterized by maxima near the stretching lineation (Figs. 8c–e). This type of quartz c-axis diagrams and the development of basal subgrain boundaries are characteristic of prism [c] slip, which is activated at high temperatures (Mainprice et al., 1986; Stipp et al., 2002). The formation of chessboard subgrains (Fig. 8a) usually takes place in the β-quartz stability field (Kruhl, 1996), which implies temperatures of ≈630 °C at pressures of 250–300 MPa. Thus, the fabric of quartz supports that the mylonitisation represents a high-temperature deformational event. The asymmetry of the diagrams points to a deformation dominated by simple shearing.

Later than the ductile shearing, many contacts between the migmatite band of the Guadaiza nappe and the peridotite massif have a long deformational history. They show a great variety of structures at successively lower temperatures to finish as fracture planes. The most significant brittle contacts are marked in the cartography of Fig. 2 as normal or reverse faults. However, the planes of mylonitic rocks deformed in ductile conditions are frequently affected by striations and slickensides indicating that they have been reactivated in brittle conditions.

4.1. Finite strain determination

In the mylonites of the Guadaiza nappe we have attempted to quantify the finite strain by using the metapelitic and quartz enclaves. The absence of planar-linear structures in the undeformed migmatites located in the lower part of the dynamothermal aureole is a limitation for the estimation of

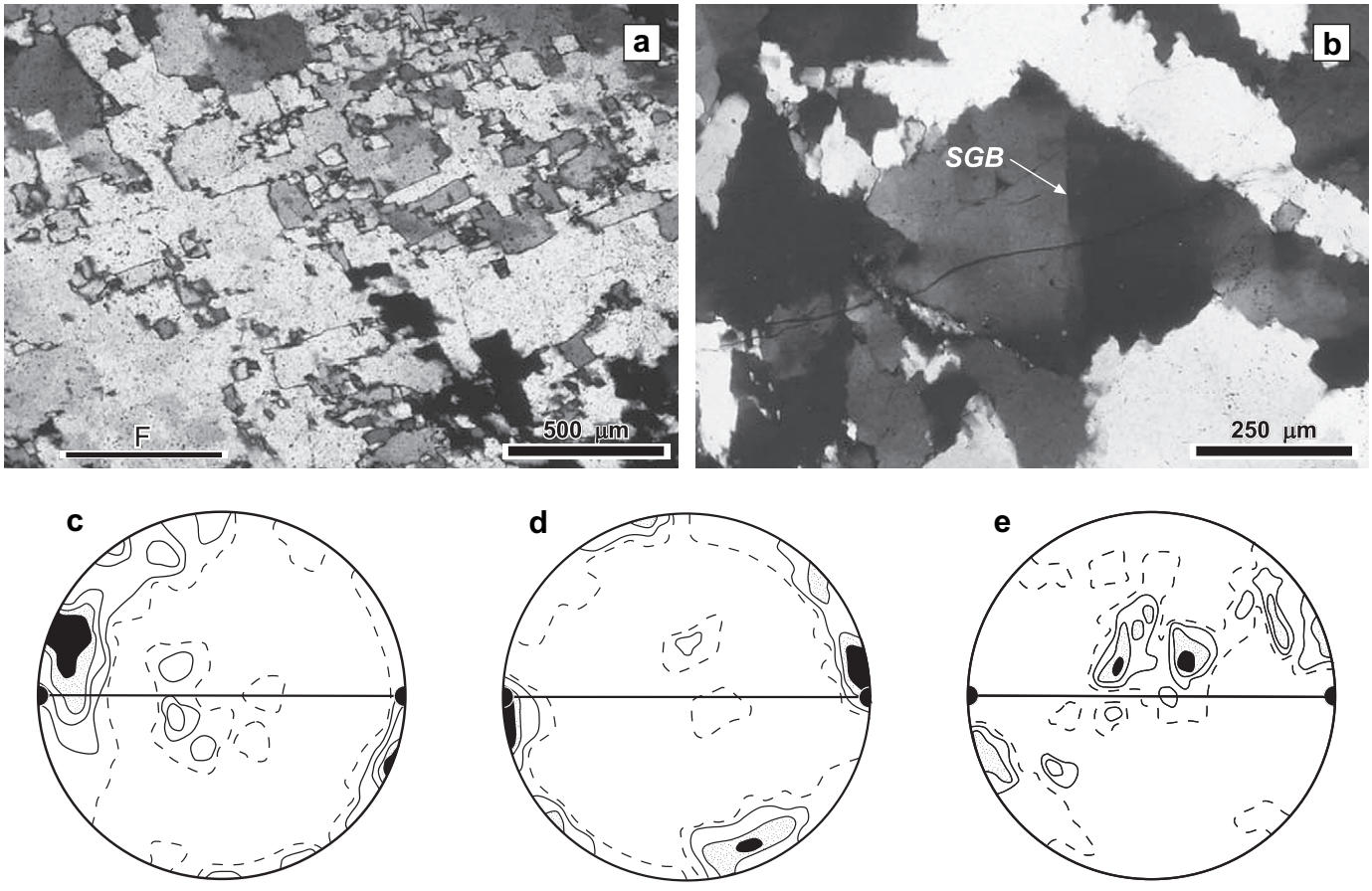

Fig. 8. (a) Quartz aggregate showing chessboard microstructure in the mylonites of the dynamothermal aureole. Note the obliquity between the mylonitic foliation (F) and the mosaic elongation. (b) Basal (0001) subgrain boundary (SGB) in quartz. Samples were cut perpendicular to the foliation and parallel to the stretching lineation. Crossed polarized light. (c, d, and e) Preferred orientation of quartz c-axes patterns in the mylonites. 150 measurements per diagram. Contours at 1, 2, 4, 6 and >8%. Diameter represents the foliation plane (XY) and black dots mark the position of the mylonitic lineation.

the original shape of the xenoliths. For this reason, we have estimated the shape of the enclaves in these undeformed rocks from two perpendicular, vertical and horizontal, sections. From the statistical point of view, undeformed enclaves of quartz show nearly spherical shapes and are represented close to the origin in the Flinn diagram. Some metapelitic enclaves have original elongated shapes, but their effects on the measurements do not distort the measurements of finite strain because the influence of the original shape of the enclaves decreases as both deformation and the number of measurements increase.

We have utilized the Flinn diagram because this representation is independent of the size of strain markers. The results presented here are based on measurements on *XZ* and *XY* sections of at least fifty markers per outcrop or thin sections from orientated samples. In order to test the influence of the lithology we have distinguished the measurements from metapelitic and quartz enclaves. Fig. 9 indicates that some measurements of the finite strain plot in the constriction field indicative of prolate ellipsoids (Flinn, 1962; Ramsay, 1967). Two outcrops located in the Guadaiza valley and in the Albornoque area (G and A, respectively on Fig. 9) provide ellipsoids on the line of plane strain of the Flinn diagram ($K = 1$) and in one outcrop the quartz enclaves are located on the flattening field. *K*-values are very similar in different outcrops, with $K = 6.56$ for most of the measured metapelitic enclaves ($X/Y = 3.56$ and $Y/Z = 1.39$) and $K = 2.95$ for the quartz ones ($X/Y = 2.65$ and $Y/Z = 1.56$).

5. Metamorphic evolution

Four samples of migmatites were analysed in order to quantify the metamorphic conditions of the dynamothermal aureole beneath the peridotites. Quantitative mineral chemical data were determined using electron microprobe analyses

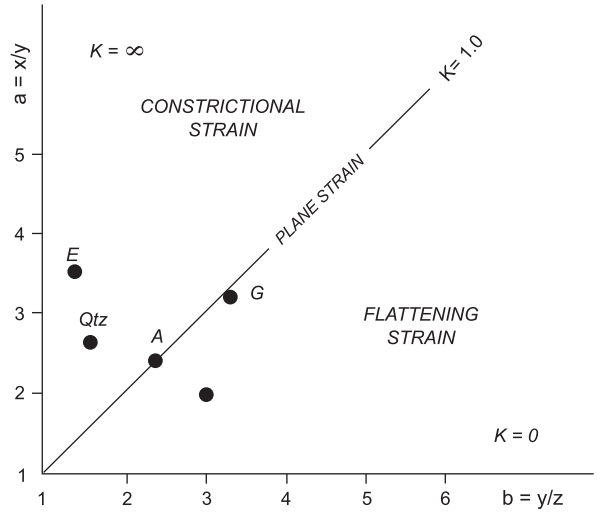

Fig. 9. Flinn diagram of the deformed xenoliths of the dynamothermal aureole. Average value of the metapelitic xenoliths (E) and quartz xenoliths (Qtz), and values of the quartz xenoliths in the Guadaiza tectonic window (G) and Albornoque area (A). The dot represented within the flattening field corresponds to quartz xenoliths in an outcrop of the Albornoque area.

(EMPA) (CAMECA SX50) with an excitation voltage of 15 kV, a beam current of 15 nA and 10 s as counting time. Total iron is presented as FeO. The average chemical compositions and the standard deviations for biotite and cordierite are represented in Table 1.

Cellular intergrowth mantles with two different compositions (An_{30} and An_{50}) around xenomorphic cores (An_{66}–An_{73}) characterize plagioclase. A thin idiomorphic zoned rim of plagioclase (An_{23}–An_{57}), which grades outward into the lowest An-contents also surrounds the grains. Cordierite appears as small inclusions in large K-feldspars or as large grains in the matrix. In this last case it is slightly pinnitized, has epitactic microstructures outlined by tiny prismatic crystals of sillimanite (Fig. 5b) and inclusions of biotite. Chemical analyses of both types of cordierites are very similar (Table 1). Sometimes cordierite replaces xenomorphic crystals of restitic andalusite (Fig. 5a). Biotite is found as inclusions within K-feldspar or cordierite and as oriented flakes parallel to the foliation of the migmatites. Few grains of garnet can be found in these rocks. They appear either as xenomorphic inclusions within K-feldspar or as xenomorphic crystals of restitic nature surrounded by biotite. Average chemical composition of garnet is $Alm_{84\text{-}74}$ $Sps_{8\text{-}3}$ $Grs_{7\text{-}0}$ $Prp_{13\text{-}6}$ $And_{6\text{-}2}$. Relict grains of andalusite are also transformed to prismatic sillimanite.

In order to determine temperature and pressure conditions, several experimentally calibrated geothermometers (Na-in-cordierite, Mirwald, 1986; Ti-in-biotite, Henry et al., 2005) and geothermobarometers (Fe–Mg exchange between cordierite-biotite, Patiño Douce et al., 1993) were applied. The problem of defining the ''effective bulk composition'' (the volume of rock in chemical equilibrium) of rocks that have suffered regional metamorphism previous to its anatexis, like it happens in the present migmatites, disable us from using the pseudosections in the calculation of pressure and temperature conditions. For this reason, we have applied alternative approaches. The mean temperature calculated using the Na-in-cordierite geothermometer for two samples (Gu-31 and Gu-37) is showed in Fig. 10. More than 160 single analyses of cordierite were done to avoid misinterpretations in the calculated temperatures. The average obtained temperatures vary from 775 ± 21 and 782 ± 21 °C (Fig. 10a). Ti-in-biotite geothermometer can also be applied to these graphite- and ilmenite-bearing peraluminous metapelites according to Henry et al. (2005) for the pressure range of 400–600 MPa. Chemical analyses of both, biotite included in cordierite and in feldspar, give a mean temperature of 725 °C (Fig. 10b; Table 1).

Since garnet is not in apparent chemical equilibrium with the minerals developed during the anatexis (K-feldspar + plagioclase + biotite + cordierite + sillimanite + tourmaline), pressure values were calculated using the second biotite solution model of Patiño Douce et al. (1993), where Fe^{3+} is ignored and biotite composition is calculated on the basis of seven (octahedral + tetrahedral) cations and a total positive charge (excluding H^+) of 22. We used 26 pairs of biotite-cordierite taking into consideration the biotites included in cordierites of the matrix. Obtained temperatures and pressures range between 678 ± 50 °C and 610 ± 76 MPa.

Table 1
Biotite and cordierite average compositions

	Biotite							Cordierite			
	Incl. in cordierite (*n*-34)		Matrix (*n*-24)		Incl. in feldspar (*n*-21)			Inclusions (*n*-10)		Matrix (*n*-40)	
	Average	St. Dev.	Average	St. Dev.	Average	St. Dev.		Average	St. Dev.	Average	St. Dev.
SiO_2	34.69	0.61	34.65	0.42	34.30	0.35	SiO_2	47.86	0.20	47.90	0.31
TiO_2	4.33	0.66	4.21	0.98	4.34	0.51	TiO_2	0.01	0.02	0.02	0.02
Al_2O_3	17.35	0.79	17.11	0.90	16.90	0.76	Al_2O_3	31.24	0.39	30.97	0.51
Cr_2O_3	0.27	0.12	0.29	0.14	0.30	0.14	Cr_2O_3	0.03	0.05	0.02	0.03
FeO	22.13	1.14	22.94	1.22	23.31	1.60	FeO	12.80	0.46	12.87	0.65
MnO	0.09	0.05	0.09	0.06	0.09	0.07	MnO	0.30	0.06	0.26	0.08
MgO	5.98	0.70	5.83	0.46	5.40	0.58	MgO	5.28	0.38	5.22	0.31
NiO	0.03	0.04	0.05	0.06	0.02	0.04	NiO	0.05	0.04	0.02	0.03
CaO	0.01	0.02	0.02	0.02	0.02	0.03	CaO	0.04	0.03	0.03	0.02
Na_2O	0.12	0.03	0.14	0.04	0.11	0.03	Na_2O	0.18	0.04	0.18	0.04
K_2O	9.27	0.27	9.46	0.23	9.29	0.24	K_2O	0.01	0.01	0.01	0.01
Σ (Ox. Range)	92.43–96.39		92.73–96.88		91.63–96.23		Σ (Ox. Range)	97.81–98.72		97.50–98.65	
Si	2.82	0.04	2.81	0.04	2.81	0.04	Si	5.06	0.01	5.08	0.02
Al^{IV}	1.18	0.04	1.19	0.04	1.19	0.04	Al	3.90	0.04	3.88	0.04
Al^{VI}	0.48	0.08	0.45	0.10	0.45	0.12	Ti	0.00	0.00	0.00	0.00
Ti	0.26	0.04	0.25	0.06	0.27	0.03	Cr	0.00	0.00	0.00	0.00
Cr	0.02	0.01	0.02	0.01	0.02	0.01	Fe^{2+}	1.13	0.04	1.14	0.06
Fe^{2+}	1.50	0.08	1.56	0.08	1.60	0.10	Mn	0.03	0.01	0.02	0.01
Mg	0.72	0.08	0.71	0.05	0.66	0.07	Mg	0.83	0.06	0.83	0.05
Mn	0.01	0.00	0.01	0.00	0.02	0.00	Ni	0.00	0.00	0.00	0.00
Ni	0.00	0.00	0.00	0.00	0.01	0.00	Ca	0.00	0.00	0.00	0.00
Ca	0.00	0.00	0.00	0.00	0.00	0.00	Na	0.04	0.01	0.04	0.01
Na	0.02	0.01	0.02	0.01	0.02	0.01	K	0.00	0.00	0.00	0.00
K	0.96	0.03	0.98	0.03	0.97	0.03	–	–	–	–	–
XMg	0.33	0.03	0.31	0.02	0.29	0.03	(Na +K)	0.04	0.01	0.04	0.01
T (°C)	725 ± 21		712 ± 50		725 ± 16		XMg	0.42	0.02	0.41	0.02

Biotite composition is calculated on basis of 11 atoms of oxygen using Laird and Albee's (1981) formulation. Crystallization temperatures for the biotite are calculated using Henry et al. (2005) geothermometer. Cordierite composition is calculated on basis of 18 atoms of oxygen.

According to previous data, the mineral paragenesis of the dynamothermal aureole does not allow us to determine the P–T conditions prior to its migmatisation process. However, owing to the preservation in the migmatites of restitic andalusite crystals replaced by cordierite (Fig. 5a) it is very likely that pre-migmatisation conditions were in the andalusite stability field, that is to say at maximum temperatures of 525–550 °C and pressures of 350–450 MPa (Fig. 11).

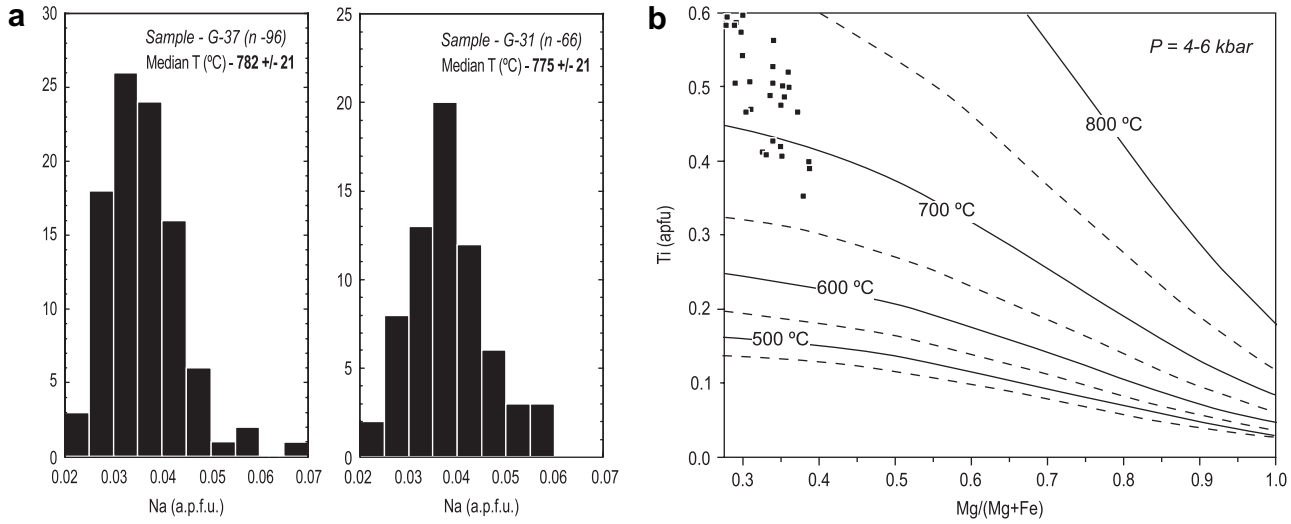

Fig. 10. (a) Na contents of cordierites of the dynamothermal aureole of Guadaiza nappe. The data are represented as histograms (frequency *vs.* Na contents in atoms per formula unit) where the crystallization temperature is given as the median temperature of all the analysed spots (n – number of analysed spots). (b) Ti *vs.* Mg/(Mg + Fe) diagram for the biotites included in cordierite and feldspar of the dynamothermal aureole. Biotite composition here is plotted on basis of 22 oxygens. Isotherms are taken from Henry et al. (2005).

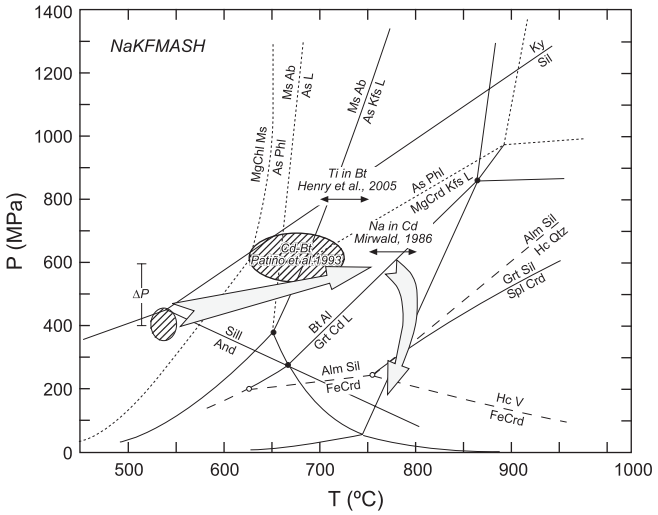

Fig. 11. Pressure-temperature-time diagram of the metamorphic evolution of the dynamothermal aureole of the Guadaiza nappe in the NaKFMASH system of Spear et al. (1999). Al_2SiO_5 triple point is taken from Pattison (1992). 1, 2 and 3 are melting reactions in pelites (see Spear et al., 1999). Calculated pressures and temperature using Patiño Douce et al. (1993; dashed ellipse), Henry et al. (2005; arrow) and Mirwald (1986; arrow) geothermobarometers are plotted in the diagram. The P–T–t path shows a clockwise cycle with a slight increase in pressure and temperature from the pre-migmatisation conditions (dashed ellipse) and a later isothermal decompression path. (Ky: kyanite, And: andalusite, Sill: sillimanite, Hc: hercynite, FeCrd: Fe-cordierite, Grt: garnet, Spl: spinel, AlSi: aluminium silicate, Phl: phlogopite, MgCrd: Mg-cordierite, Kfs: K-feldspar, V: H_2O, L: liquid).

Published P–T data from the underlying schists of the Guadaiza nappe are consistent with this interpretation (Tubía, 1988). The metapelitic solidus in the NaKFMASH system of Spear et al. (1999) and the assemblage defined by cordierite-K-feldspar-biotite-sillimanite-quartz in absence of garnet in chemical equilibrium establishes a new temperature range of 675–750 °C for the migmatisation in agreement with previous geothermometric calculations (Fig. 11). The pressure conditions at which the migmatisation took place are poorly constrained. Previously published pressure values vary between 350 and 610 MPa (Loomis, 1972; Torres-Roldán, 1983; Argles, 1996; this work). We consider that the higher values are more consistent with the regional tectonic data, because the emplacement of all the Los Reales nappe and the Malaguide Complex sequence over the Guadaiza nappe must have generated a significant pressure increase induced by the loading of a ≈7 km thick column of rocks equivalent to 200 MPa. Thus, starting from the 350–450 MPa established for the pre-migmatisation stage, a pressure range of 550–650 MPa for the migmatisation is a more realistic estimation. The most probable P–T path for the dynamothermal aureole (Fig. 11) involves a clockwise cycle with a slight increase in pressure during the migmatisation and followed by decreasing pressures at constant temperature stated by the garnet + sillimanite = spinel + cordierite + quartz reactions recorded in the enclaves of the dynamothermal aureole.

6. Discussion

A significant feature in the Guadaiza nappe is that two different episodes of migmatisation have been recorded (Fig. 3). The older one is of Hercynian age and represented by the Istan migmatites. It is followed by the migmatites related to the dynamothermal aureole that clearly cut the overall lithological sequence of the Guadaiza nappe, from the uppermost marbles located at the southern part of the Guadaiza window to the Istan migmatites in the Albornoque sector (see the map of Fig. 2). The migmatite band generated around the peridotite contact shows the characteristics of a dynamothermal aureole formed by the anatexis of the rocks of the Guadaiza nappe. This anatexis increases towards the peridotite contact, producing a granite rock with phenocrysts of cordierite and K-feldspar and numerous schist restites, resisters of quartzite, marble or quartz and even xenoliths of peridotites. The sheeted geometry of the dynamothermal aureole, its obliquity to the regional schistosity of the Guadaiza schists and brown quartzites and the concordance with the basal contact of the Ronda peridotites (Fig. 2) supports an interpretation whereby different portions of the Guadaiza nappe sequence experienced partial melting during the tectonic emplacement of the overlying Ronda peridotites.

Starting with maximum temperatures of 525–550 °C before the migmatisation, a minimum temperature increase of 125 °C is needed to produce partial melts from the mica-bearing schists of the Guadaiza nappe. Among the ways in which crustal rocks can be heated in active collisional orogens, radiogenic decay of the crust, heating from convective upwelling asthenosphere and dissipative heating associated to shear zones are particularly relevant (England and Molnar, 1993). An acceptable model for the origin of the Guadaiza dynamothermal aureole should integrate these restrictions imposed by the data:

1) There is an apparent inverted metamorphism, as the migmatites of the aureole rest over schists of lower metamorphic grade.
2) Mylonitisation took place at very high-temperature conditions, $T > 630$ °C, close to the metapelitic solidus in the NaKFMASH system.
3) Restitic andalusite crystals armoured by cordierite indicate that the development of the aureole postdates – or is coeval to – the late Miocene thermal metamorphism.
4) The peridotite sheet was hot during its emplacement over the Guadaiza nappe. Temperatures of 1060 ± 15 °C have been estimated for the plagioclase peridotites (Remaïdi, 1993) that have been related to the ductile emplacement of the Ronda peridotites into the crust (Van der Wal and Vissers, 1996).

The main thermal budget, up to 550 °C, probably reflects the delayed heating due to the thermal metamorphism recognized elsewhere in the Alpujarride Complex. This event is associated with a late thermal pulse from upwelling asthenosphere replacing the (removed) lithospheric root formed

during the Mesozoic to Tertiary convergence between the African and Iberian plates (Platt and Vissers, 1989). However, the inverted metamorphism requires the conduction of heat downwards. In the present case, this could be due to the fast emplacement of a hot peridotite slab of some 4 km thick, combined with the transient dissipative heating generated by the motion on the ductile shear zone between the peridotite and the Guadaiza nappe.

There are few data on the age of episodes in the history of the Guadaiza rocks. As stated in the Section 3, the regional metamorphism was dated as Hercynian (Acosta, 1997; Sánchez Rodríguez, 1998). The formation of the dynamothermal aureole in Miocene times is well constrained by the granite dykes that emanated from the aureole and intruded the overlying peridotites (Cuevas et al., 2006). Recent U/Pb SHRIMP dating of zircons from such granite dykes have provided ages of 18.8 ± 4.9 Ma (Sánchez Rodríguez and Gebauer, 2000) or 21.8 ± 0.5 Ma (Esteban et al., 2007).

Strain in ductile shear zones is frequently explained by an ideal pattern of homogeneous shearing (Ramsay and Graham, 1970; Ramsay, 1980). This pattern considers that the ductile shear zone is confined between rigid walls that only experience relative displacements parallel to each other. Consequently, the strain is produced by simple shear and requires a plane deformation. However, as natural shear zones only rarely meet such ideal conditions more complex patterns on the kinematic evolution of ductile shear zones have been elaborated (Sanderson and Marchini, 1984; Robin and Cruden, 1994; Hudleston, 1999). Data obtained from the mylonitic rocks of the dynamothermal aureole of the Guadaiza nappe (Fig. 9) suggest that one part of the deformation is produced by simple shear conditions (in the plane deformational field), but other data reflect a regime in the constrictional field, with linear tectonites where $L > S$, and there is some evidence for a regime of deformation in the flattening field, with planar-linear tectonites where $L = S$. Another remarkable point is that the mineral associations in the analysed samples are similar, suggesting that these different deformational regimes operate simultaneously in diverse zones.

The overall structure of this composite shear zone can be described as a heterogeneous system with three layers of contrasting rheological behaviours, since the magma-rich dynamothermal aureole acted like a low-viscosity channel confined between harder materials, corresponding to the overlying slab of peridotites and the underlying schists and brown quartzites of the Guadaiza nappe. Flow in the low viscosity crustal channel of the Himalayan-Tibetan orogen is partitioned into eastward and southward trends (Beaumont et al., 2001; Harris, 2007). Although at different scale, the fan-like pattern shown by the trend of stretching lineations in the mylonites (Fig. 7) can be interpreted in a similar way: dominant N10°W trending lineations would mark the emplacement direction of the peridotite slab, while E-ward trending lineations could be related to the lateral flow of the low-viscosity aureole due to lithostatic loading induced by the harder hangingwall plate.

The thinness of the mylonitic zone (≈ 30 m) can be attributed to the low viscosity of the materials due to the high temperatures and to generalized presence of melts. The production of dissipative heat practically ceases once melts concentrate along a shear zone, as shear stress drops dramatically. A transient temperature reduction would favour the crystallization of melts and the development of high-temperature solid-state deformation. In turn, the crystallization and deformation will promote a new cycle of dissipative heating. It is worth noting that such a valve effect of the shear-heating can explain the interplay between melting and high-temperature deformation processes evidenced here. These conditions favour the localization of the strain due to thermal and melt-enhanced weakening. Shearing hampered the rise of magmas through the high strain zone trapping them as sheeted intrusions concordant to the mylonite band. Some evidence of mass transfer to the upper border of the mylonite zone, such as the granite dyke intrusions in the Sierra Bermeja peridotite massif, is recognized (Cuevas et al., 2006). Finally, the build-up of granite magmas generated the brecciation due to melt-enhanced embrittlement processes. This process explains the generation of xenoliths and the roughly coeval escape of granite magmas that intrude as dykes in the overlying peridotites. The interaction of transient periods dominated by melt-enhanced ductile deformation and melt-enhanced embrittlement could explain the heterogeneity of the shear zone.

From the regional point of view, the heterogeneous nature of strain in the mylonites of the dynamothermal aureole in the Guadaiza nappe has important kinematic implications because the stretching lineation can form at a high angle to the general orientation of movement in the shear zone (Robin and Cruden, 1994; Passchier, 1998). The fan-like distribution of the stretching lineation around N10°W can be explained by periods when the magma was more abundant, and a non-linear flow in the foliation planes predominated. This is due to the low viscosity of the composite melt-solid framework system. The angular deviation between the stretching lineation and the movement orientation only occurs in minor shear zones where finite strain is in the apparent constriction field (Hudleston, 1999). In the mylonites of the dynamothermal aureole the samples with stretching lineation directed NW–SE and NE–SW have K values higher than 1. This is the reason why we have considered that the more representative direction for the relative motion between the Guadaiza and Los Reales nappe is NNW.

From the tectonic point of view, Alpine orogenesis of the Betic Cordilleras resulted from the collision of the African and Iberian plates and is currently interpreted in terms of two main phases: an early event of lithospheric shortening was succeeded by the Miocene extension of the Internal Zone of the orogen (Platt and Vissers, 1989; Monié et al., 1994; Tubía, 1994; Zeck, 1996; Sánchez Rodríguez and Gebauer, 2000). The subcontinental mantle was involved in the nappe stacking, as is evidenced by the presence of the Ronda peridotites at the base of the structurally highest nappe, the so-called Los Reales nappe, of the Alpujarride complex of the Internal Zone (Tubía et al., 1992). The age of lithospheric shortening is not yet well constrained, since radiometric ages commonly record late thermal events coeval with the

subsequent extension of the orogen (see Esteban et al., 2004 and references therein).

7. Conclusions

The structural study compiled here deals with the evolution and kinematics of the basal dynamothermal aureole of the Ronda peridotites, located in the Sierra Bermeja massif of the Western Betic Cordilleras. This dynamothermal aureole developed as a melt-bearing shear zone. The main concluding remarks of this work can be summarized as follows:

- This dynamothermal aureole is characterized by a marked strain gradient towards the contact with the overlying peridotites, a great angular dispersion, $\approx 90^{\circ}$, of stretching lineations and the intrusion of thin granite sheets coeval with the deformation.
- These features are consistent with the aureole being a low-viscosity shear zone formed at temperatures high enough, $>650\,^{\circ}C$, to promote the partial melting of crustal metamorphic rocks. We consider that the heat source came from the hot emplacement of the Ronda peridotites, the dissipative heating produced by the shear zone and the delayed latent heat due to the Miocene thermal metamorphism.
- The interaction of alternating events of melt-enhanced deformation and melt-enhanced embrittlement explains the heterogeneity of this ductile shear zone and the strong narrowing, only 30 meters of mylonitic rocks, of the deformed domain.
- Our results indicate that under temperatures high enough to promote partial melting of continental crustal rocks, ductile shear zones can experience a dramatic narrowing instead of the broadening suggested for increasing depth (and temperature) in the widely accepted model of Sibson (1977).

Acknowledgements

This work was supported by the Ministerio de Ciencia y Tecnología (CGL2004-00701 and CGL2007-60030/BTE) and the Universidad del País Vasco (Spain). The carefully reviews of Tom Argles and an anonymous reviewer have contributed to improve the original version of the manuscript.

References

Acosta, A., 1997. Estudio de los fenómenos de fusión cortical y generación de granitoides asociados a las peridotitas de Ronda. Ph.D. thesis, University of Granada.

Argles, T., 1996. Tectonometamorphic studies in the crustal envelope of mantle peridotites in the Western Betic Cordillera, Southern Spain. Ph.D. thesis, University of Oxford.

Beaumont, C., Jamieson, R.A., Nguyen, M.H., Lee, B., 2001. Himalayan tectonics explained by extrusion of a low-viscosity crustal channel coupled to focused surface denudation. Nature 14, 738–742.

Blenkinsop, T., 2000. Deformation. Microstructures and Mechanisms in Minerals and Rocks. Kluwer Academic Publishers, Dordrecht.

Brown, M., Solar, G.S., 1998. Shear zones and melts: positive feedback in orogenic belts. Journal of Structural Geology 20, 211–227.

Cuevas, J., Esteban, J.J., Tubía, J.M., 2006. Tectonic implications of the granite dyke swarm in the Ronda peridotites (Betic Cordilleras, Southern Spain). Journal of the Geological Society, London 163, 631–640.

Davidson, C., Schmid, S.M., Hollister, L.S., 1994. Role of melt during deformation in the deep crust. Terra Nova 6, 133–142.

Dewey, J.F., Helmann, M.L., Turco, E., Hutton, D.H.W., Knott, S.D., 1989. Kinematics of the western Mediterranean. In: Coward, M.P., Dietrich, D., Park, R.G. (Eds.), Alpine Tectonics. Special Publications, vol. 45. Geological Society, London, pp. 265–283.

Egeler, C.G., Simon, O.J., 1969. Sur la tectonique de la Zone Bétique (Cordillères Bétiques, Espagne). Verhandelingen der Koninklijke Nederlands Akademie van Wetenschappen. Natuurkunde 25.

England, P., Molnar, P., 1993. The interpretation of inverted metamorphic isograds using simple physical calculations. Tectonics 12, 145–157.

Esteban, J.J., Sánchez-Rodríguez, L., Seward, D., Cuevas, J., Tubía, J.M., 2004. The late thermal history of the Ronda area. Tectonophysics 389, 81–92.

Esteban, J.J., Cuevas, J., Tubía, J.M., Liati, A., Seward, D., Gebauer, D., 2007. Timing and origin of zircon-bearing chlorite schists in the Ronda peridotites (Betic Cordilleras, Southern Spain). Lithos 99, 121–135.

Flinn, D., 1962. On folding during the three-dimensional progressive deformation. Journal of the Geological Society, London 118, 385–433.

Harris, N., 2007. Channel flow and the Himalayan-Tibetan orogen: a critical review. Journal of the Geological Society, London 164, 511–523.

Henry, D.J., Guidotti, C.V., Thomson, J.A., 2005. The Ti-saturation surface for low-to-medium pressure metapelitic biotites: implications for geothermometry and Ti-substitution mechanisms. American Mineralogist 90, 316–328.

Hollister, L.S., Crawford, M.L., 1986. Melt-enhanced deformation: a major tectonic process. Geology 14, 558–561.

Hopgood, A.M., 1999. Determination of Structural Successions in Migmatites and Gneisses. Kluwer Academic Publishers, Dordrecht.

Hudleston, P., 1999. Strain compatibility and shear zones: is there a problem? Journal of Structural Geology 21, 923–932.

Katz, R.F., Spiegelman, M., Holtzman, B., 2006. The dynamics of melt and shear localization in partially molten aggregates. Nature 442, 676–679.

Kruhl, J.H., 1996. Prism- and basal-plane parallel subgrain boundaries in quartz: a microstructural geothermobarometer. Journal of Metamorphic Geology 14, 581–589.

Laird, J., Albee, A.L., 1981. High-Pressure metamorphism in mafic schist from Northern Vermont. American Journal of Science 281, 97–126.

Loomis, T.P., 1972. Contact Metamorphism of pelitic rock by the Ronda Ultramafic intrusion, Southern Spain. Geological Society of America Bulletin 83, 2449–2473.

Lundeen, M.T., 1978. Emplacement of the Ronda peridotite, Sierra Bermeja, Spain. Geological Society of America Bulletin 89, 172–180.

Mainprice, D., Bouchez, J.L., Blumenfeld, Ph., Tubía, J.M., 1986. Dominant *c* slip in naturally deformed quartz: implications for dramatic plastic softening at high temperature. Geology 14, 819–822.

Mancktelow, N.S., 2006. How ductile are ductile shear zones? Geology 34, 345–348.

Mirwald, P.W., 1986. Ist cordierit ein geothermometer? Fortschritte der Mineral 64, 119.

Monié, P., Torres-Roldán, R.L., García-Casco, A., 1994. Cooling and exhumation of the Western Betic Cordilleras, $^{40}Ar/^{39}Ar$ thermochronological constraints on a collapsed terrane. Tectonophysics 238, 353–379.

Navarro-Vilá, F., Tubía, J.M., 1983. Essai d'une nouvelle differentiation des Nappes Alpujarrides dans le secteur occidental des Cordillères Bétiques (Andalousie, Espagne). Comptes Rendues de l'Académie des Sciences 296, 111–114.

Obata, M., 1980. The Ronda peridotite: garnet-, spinel-, and plagioclase-lherzolite facies and the P–T trajectories of a high temperature mantle intrusion. Journal of Petrology 21, 533–572.

Passchier, C.W., 1986. Flow in natural shear zones: the consequences of spinning flow regimes. Earth and Planetary Science Letters 77, 70–80.

Passchier, C.W., 1998. Monoclinic model shear zones. Journal of Structural Geology 20, 1121–1137.

Patiño Douce, A.E., Johnston, A.D., Rice, J.M., 1993. Octahedral excess mixing properties in biotite – a working model with applications to geobarometry and geothermometry. American Mineralogist 78, 113–131.

Pattison, D.R.M., 1992. Stability of andalusite and sillimanite and the Al_2SiO_5 triple point: constraints from the Ballachulish aureole, Scotland. Journal of Geology 100, 423–446.

Platt, J.P., Behrmann, J.H., 1986. Structures and fabrics in a crustal-scale shear zone, Betic Cordillera, SE Spain. Journal of Structural Geology 8, 15–33.

Platt, J.P., Vissers, R.L.M., 1989. Extensional collapse of thickened continental lithosphere – a working hypothesis for the Alboran Sea and Gibraltar Arc. Geology 17, 540–543.

Ramsay, J.G., 1967. Folding and Fracturing of Rocks. MacGraw-Hill, New York.

Ramsay, J.G., 1980. Shear zone geometry: a review. Journal of Structural Geology 2, 83–99.

Ramsay, J.G., Graham, R.D., 1970. Strain variation in shear belts. Canadian Journal of Earth Sciences 7, 786–813.

Remaïdi, M., 1993. Etude pétrologique et géochimique d'une association péridotites réfractaires-pyroxénites dans le massif de Ronda (Espagne). Ph. D. thesis, University of Montpellier II.

Robin, P.Y., Cruden, A.R., 1994. Strain and vorticity patterns in ideally ductile transpression zones. Journal of Structural Geology 16, 447–466.

Rutter, E.H., Holdsworth, R.E., Knipe, R.J., 2001. The nature and tectonic significance of fault-zone weakening: an introduction. In: Holdsworth, R.E., Strachan, R.A., Macgoughlin, J.F., Knipe, R.J. (Eds.), The Nature and Tectonic Significance of Fault-zone Weakening. Special Publications, vol. 186. Geological Society, London, pp. 1–11.

Sánchez Rodríguez, L., 1998. Pre-Alpine and Alpine evolution of the Ronda Ultramafic Complex and its country-rocks (Betic chain, southern Spain): U-Pb SHRIMP zircon and fission-track dating. Ph. D. thesis, Swiss Federal Institute of Technology Zürich.

Sánchez Rodríguez, L., Gebauer, D., 2000. Mesozoic formation of pyroxenites and gabbros in the Ronda area (southern Spain), followed by Early Miocene subduction metamorphism and emplacement into the middle crust: U-Pb sensitive high-resolution ion microprobe dating of zircon. Tectonophysics 316, 19–44.

Sanderson, D.J., Marchini, W.R., 1984. Transpression. Journal of Structural Geology 6, 449–458.

Sibson, R.H., 1977. Fault rocks and fault mechanisms. Journal of the Geological Society, London 133, 191–213.

Spear, F.S., Kohn, M.J., Cheney, J.T., 1999. P–T paths from anatectic pelites. Contributions to Mineralogy and Petrology 134, 17–32.

Stipp, M., Stünitz, H., Heilbronner, R., Schmid, S.M., 2002. The eastern Tonale fault zone: a ''natural laboratory'' for crystal plastic deformation of quartz over a temperature range from 250 to 700 °C. Journal of Structural Geology 24, 1861–1884.

Torres-Roldán, R.L., 1983. Fractionated melting of metapelite and further crystal-melt equilibria – the example of the Blanca Unit Migmatite Complex, North of Estepona (Southern Spain). Tectonophysics 96, 95–123.

Tubía, J.M., 1988. Estructura de los Alpujárrides occidentales: cinemática y condiciones de emplazamiento de las peridotitas de Ronda. Publicaciones especiales del Boletín Geológico y Minero 99, 1–124.

Tubía, J.M., 1994. The Ronda Peridotites (Los Reales Nappe) – an example of the relationship between lithospheric thickening by oblique tectonics and late extensional deformation within the Betic-Cordillera (Spain). Tectonophysics 238, 381–398.

Tubía, J.M., Cuevas, J., 1986. High-temperature emplacement of the Los Reales peridotite nappe (Betic Cordillera, Spain). Journal of Structural Geology 8, 473–482.

Tubía, J.M., Gil Ibarguchi, J.I., 1991. Eclogites of the Ojen nappe: a record of subduction in the Alpujarride complex (Betic Cordilleras, southern Spain). Journal of the Geological Society, London 148, 801–804.

Tubía, J.M., Cuevas, J., Navarro-Vilá, F., Alvarez, F., Aldaya, F., 1992. Tectonic evolution of the Alpujarride Complex (Betic Cordilleras, southern Spain). Journal of Structural Geology 14, 193–203.

Tubía, J.M., Cuevas, J., Gil Ibarguchi, J.I., 1997. Sequential development of the metamorphic aureole beneath the Ronda peridotites and its bearing on the tectonic evolution of the Betic Cordillera. Tectonophysics 279, 227–252.

Van der Molen, I., Paterson, M.S., 1979. Experimental deformation of partially-melted granite. Contributions to Mineralogy and Petrology 70, 229–318.

Van der Wal, D., Vissers, R.L.M., 1996. Structural petrology of the Ronda peridotite, SW Spain: deformation history. Journal of Petrology 37, 23–43.

Zeck, H.P., 1996. Betic-Rif orogeny: subduction of Mesozoic Tethys lithosphere under eastward drifting Iberia, slab detachment shortly before 22 Ma, and subsequent uplift and extensional tectonics. Tectonophysics 254, 1–16.